Modeling of LiFePO4 battery open circuit voltage hysteresis based on recursive discrete Preisach model*

Wei-Yi Sun(孙维毅)[1], Hai-Tao Min(闵海涛)[1], Dong-Ni Guo(郭冬妮)[2], and Yuan-Bin Yu(于远彬)[1,†]

[1] *State Key Laboratory of Automotive Simulation and Control, Jilin University, Changchun* 130022, *China*
[2] *China FAW Group Corporation R & D Center, Changchun* 130011, *China*

(Received 18 June 2017; revised manuscript received 4 September 2017; published online 20 November 2017)

This paper focuses on the modeling of LiFePO4 battery open circuit voltage (*OCV*) hysteresis. There exists obvious hysteresis in LiFePO4 battery *OCV*, which makes it complicated to model the LiFePO4 battery. In this paper, the recursive discrete Preisach model (RDPM) is applied to the modeling of LiFePO4 battery *OCV* hysteresis. The theory of RDPM is illustrated in detail and the RDPM on LiFePO4 battery *OCV* hysteresis modeling is verified in experiment. The robust of RDPM under different working conditions are also demonstrated in simulation and experiment. The simulation and experimental results show that the proposed method can significantly improve the accuracy of LiFePO4 battery *OCV* hysteresis modeling when the battery *OCV* characteristic changes, which conduces to the online state estimation of LiFePO4 battery.

Keywords: hysteresis, lithium–ion batteries, modeling

PACS: 75.60.Ej, 82.47.Aa, 47.50.Cd **DOI:** 10.1088/1674-1056/26/12/127503

1. Introduction

In recent years, electric vehicles (EVs) have been more and more popular due to the advantages of zero pollution and high energy efficiency.[1–3] Li–ion batteries are considered to be the most promising energy storage system to meet the specific energy and power demands of EVs, which has high energy density, good cycle-life performance, and low self-discharge rate.[4–10] LiFePO4 battery is one of the most promising solutions for EV energy storage system with the benefits of excellent thermal stability and low cost. As a crucial characteristic relationship, the state of charge (*SOC*)–*OCV* relationship plays an important role in EV battery manage system (BMS). However, there exhibits a pronounced hysteresis between the *SOC*–*OCV* relationship of LiFePO4 battery.[11] The existence of hysteresis means that the *SOC*–*OCV* curve is not a one-to-one mapping but the *OCV* value varies at the same *SOC* point between charge and discharge. This special characteristic makes it difficult to accurately model the *SOC*–*OCV* relationship of LiFePO4 battery.

There have been extensive studies dealing with battery hysteresis modeling.[12–25] The Preisach model (PM) is one of the most popular methods for battery hysteresis modeling. The Preisach model was proposed by Preisach[21] in 1935 and has been used for hysteresis modeling in various kinds of systems such as magnetics, piezoelectric actuators, batteries, etc. In Ref. [22], the discrete Preisach model was used to describe the *OCV* hysteresis for NiMH battery. In Ref. [23], the same approach was applied to the *OCV* hysteresis modeling of LiFePO4 battery. In Refs. [22] and [23], the discrete Preisach model worked effectively both for NiMH battery and LiFePO4 battery. In Ref. [24], the Everett function was adopted to discretize the Preisach model, and the first-order reversal branch test was used to identify the density function, which simplifies the measurement and reduces the computation resources. In Ref. [25], an adaptive discrete Preisach model is used to model the hysteresis of LiFePO4 battery.

It is noticeable that the battery parameters are subjected to change due to different working and aging conditions, which means that the *SOC*–*OCV* model works in a certain condition may not work well in another condition. This phenomenon makes it necessary to build a model that can be adapted to the change of the hysteresis characteristic of LiFePO4 battery. However, this problem has rarely been discussed in existing researches. As a main contribution of this paper, an *SOC*–*OCV* modeling method that can be adapted to the change of battery *OCV* characteristic is proposed based on the recursive discrete Preisach model. The rest of this paper is organized as follows. In Section 2 the method of the paper is described including a detailed introduction to the classical Preisach model (CPM) and the proposed RDPM algorithm. In Section 3, the experimental test bench is introduced and the Preisach density function (PDF) of two different LiFePO4 cells are tested in experiment. In Section 4 the effectiveness of RDPM is validated and the performances of RDPM under different working conditions are validated. Finally, some conclusions are drawn from the present study in Section 5.

*Project supported by the National Natural Science Foundation of China (Grant No. 51107052).
†Corresponding author. E-mail: yyb@jlu.edu.cn
© 2017 Chinese Physical Society and IOP Publishing Ltd

2. Method

2.1. Classical Preisach model

The classical Preisach model is defined as an infinite collection of ideal relay operators as shown in Fig. 1. The states of the relay operators are assumed to switch between "'up"' (+1) and "'down"' (−1) according to the input. The relationship of the input value and the states of relay operators can be described as

$$\gamma_{\alpha\beta}[u(t)] = \begin{cases} 1, & u(t) > \alpha, \\ \text{remain unchangesd}, & \alpha \le u(t) \le \beta, \\ -1, & u(t) < \beta, \end{cases} \quad (1)$$

where $\gamma_{\alpha\beta}[\cdot]$ is the relay operator, $u(t)$ is the input at time t, α is the switch-up value, and β is the switch-down value.

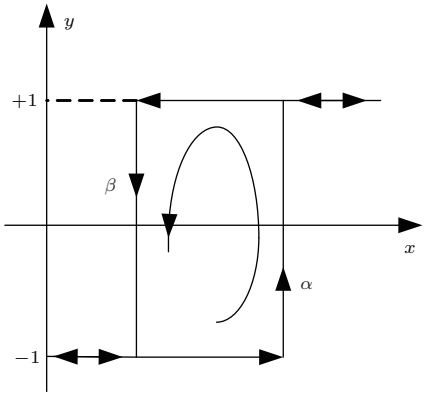


Fig. 1. Ideal relay operator.

And the Preisach model is defined as

$$y(t) = \iint_{\alpha\ge\beta} \mu(\alpha,\beta)\,\gamma_{\alpha\beta}[u(t)]\,\mathrm{d}\alpha\mathrm{d}\beta, \quad (2)$$

where $y(t)$ denotes the output at time t, and $\mu(\alpha,\beta)$ is the density function of the relay operator at the position of $(\alpha\beta)$.

In practical cases, the threshold of α and β is limited by the value of $u(t)$, so the integration domain can be restricted to a triangular domain, which is defined as the Preisach triangle. As illustrated in Fig. 2, the horizontal axis represents the switch-down value and the vertical axis is the switch-up value. The values of $u_{\min}$ and $u_{\max}$ are the boundary of the input value. Then the Preisach model can be rewritten as

$$y(t) = \iint_{T} \mu(\alpha,\beta)\,\gamma_{\alpha\beta}[u(t)]\,\mathrm{d}\alpha\mathrm{d}\beta, \quad (3)$$

The characteristic of the Preisach operator enables the Preisach model to memorize the historical paths of the input. The history of the input can be represented in the Preisach triangle by a staircase line $L(t)$, which is composed of horizontal and vertical line(s). Each segment corresponds to a rising or falling part of the input history. For the increasing input, the memory curve is horizontal and moves up towards the local maximum value along the vertical axis; for the decreasing input, the memory curve becomes vertical and moves towards the local minimum value along axis β. With the rising and falling of the input values, new extrema are produced consistently and old extrema are replaced by the new ones if the input exceeds the old extrema.[26]

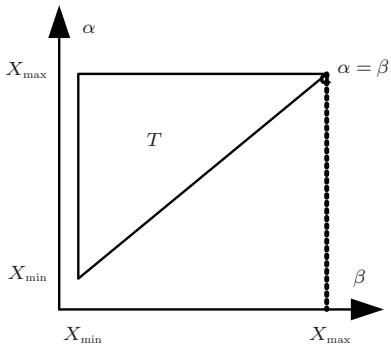


Fig. 2. Preisach triangle.

As shown in Fig. 3, the memory curve L subdivides the Preisach plane into two regions i.e., region P^+ and region P^-. Region P^+ contains the relay operators with the "'up"' state, and region P^- contains the relay operators with the "'down"' state. According to the definition of relay operator, it is easy to know that the values of $\gamma_{\alpha\beta}[u(t)]$ are -1 in the area P−, and $+1$ in the area of P+, respectively so equation (3) can be rewritten as

$$\begin{aligned} y(t) &= \iint_{P}^{+} \mu(\alpha,\beta)\,\mathrm{d}\alpha\mathrm{d}\beta - \iint_{P}^{-} \mu(\alpha,\beta)\,\mathrm{d}\alpha\mathrm{d}\beta \\ &= 2\iint_{P}^{+} \mu(\alpha,\beta)\,\mathrm{d}\alpha\mathrm{d}\beta - \iint_{T} \mu(\alpha,\beta)\,\mathrm{d}\alpha\mathrm{d}\beta. \end{aligned} \quad (4)$$

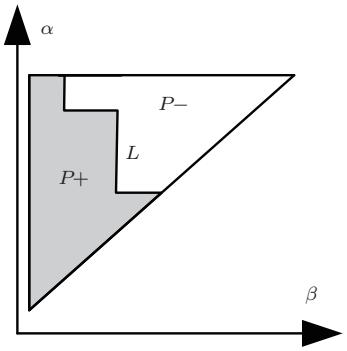


Fig. 3. Memory curve L subdividing the Preisach plane into regions P^+ and P^-.

2.2. Recursive discrete Preisach model

To calculate the output of the Preisach function, the weight function $\mu(\alpha,\beta)$ must be identified. However, it is hard to identify the value of the continuously distributed relay operators. To solve this problem, usually a uniform discretization step is involved to discretize the continuous Preisach operator into a finite dimensional model.[22] As shown in Fig. 4, both legs of the Preisach triangle ranging from $u_{\min}$ and $u_{\max}$ are equally divided into N parts (say, $N = 4$), thus the Preisach triangle is divided by uniform lattice cells and the weight function $\mu(\alpha,\beta)$ is approximated by a piecewise constant function $\omega(\alpha,\beta)$. For the convenience of computation and without loss of generality, the area of each square cell is set as unit one, i.e.

$\mathrm{d}\alpha = 1$ and $\mathrm{d}\beta = 1$. Then the Preisach function of Eq. (4) can be further written as

$$y(t) = 2\sum_{P^+(t)} \omega(\alpha,\beta) - \varepsilon_0, \tag{5}$$

where $\varepsilon_0 = \iint_T \mu(\alpha,\beta)\,\mathrm{d}\alpha\mathrm{d}\beta$ and $\sum_{P^+(t)}$ represents the sum of the values of all the cells in the area of P^+ at time t.

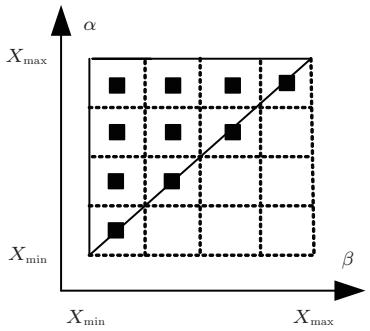


Fig. 4. Discrete Preisach plain.

As mentioned in the Introduction, the characteristic of the battery changes under different working and aging conditions. To solve this problem, an online *SOC–OCV* modeling algorithm should be adopted. Inspired by the work of Ruderman M *et al.*,[27] a recursive discrete Preisach model is adopted in this paper. The main difference between CPM and RDPM is that in RDPM the Preisach density function is identified online based on the output increment error As shown in Fig. 5, assume $u(t)$ and $u(t+1)$ to be two consecutive inputs, the corresponding outputs are $y(t)$ and $y(t+1)$ respectively, then the corresponding output increment will be calculated as

$$\begin{aligned}\Delta y &= y(t+1) - y(t)\\ &= 2\sum_{P^+(t+1)} \omega(\alpha,\beta) - 2\sum_{P^+(t)} \omega(\alpha,\beta)\\ &= 2\sum_{\Omega} \omega(\alpha,\beta).\end{aligned} \tag{6}$$

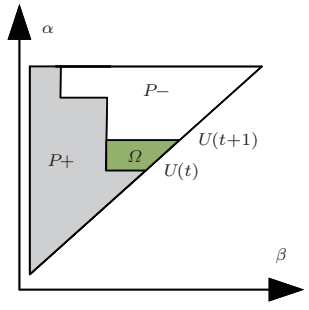


Fig. 5. (color online) Input and output increases.

From Eq. (6) it can be seen that the increase of the output only relates to the relay operators in polygon Ω, which is composed of the relay operators that experience a state transition from the "up" to the "down" state between $u(t)$ and $u(t+1)$. Assume that the estimated $\hat{\omega}(\alpha\beta)$ does not coincide with the true $\omega(\alpha,\beta)$ value, then there will exist a deviation between the real and modeled output increment, which can be expressed as

$$e = \Delta y - \Delta\hat{y} = 2\sum_{\Omega}[\omega(\alpha,\beta) - \hat{\omega}(\alpha,\beta)]. \tag{7}$$

It is evident that the error increase relates to the difference between ω_Ω and $\hat{\omega}_\Omega$ and is zero in the case $\omega_\Omega = \hat{\omega}_\Omega$. For each $\omega_\Omega \in \Omega$ the update is defined as

$$\hat{\omega}_\Omega(t+1) = \hat{\omega}_\Omega(t) + \frac{e}{A_\Omega}, \tag{8}$$

where A_Ω is the total area of the switching polygon. Then the Preisach model can be updated according to Eq. (8). Comparing with the update scheme in ADPM,[25] the key difference in this work is that only the hysterons contributing directly to the output deviation is updated, instead of updating every hysteron in each step.

3. Experiment

3.1. Test bench construction

The experimental setup consists of (i) LiFePO4 test cells, (ii) chroma 72001 battery test system, (iii) a host computer, and (iv) a thermal chamber. Two LiFePO4 test cells are used and the details are given in Table 1. The chroma 72001 battery test system is used to charge and discharge the battery with a maximum voltage of 5 V and a maximum current of 20 A at an accuracy of 1-mV voltage and 10-mA current. The thermal chamber is used to maintain the environment temperature of the experiments. The experimental data such as current and voltage are measured by the Chroma 72001 and recorded by the host computer.

Table 1. Details of cells used.

	Cell A	Cell B
Manufacturer	LS	BAK
Cell name	LR18650EC	BDL26650
Negative electrode	C	C
Positive electrode	LiFePO4	LiFePO4
Nominal capacity/Ah	1.7	3.0
Nominal voltage/V	3.2	3.2
Charge cutoff voltage/V	3.65	3.65
Discharge cutoff voltage/V	2.0	2.0

3.2. PDF identification

Pulse current tests (PCTs) are carried out to measure the OCVs of the battery at different SOCs. As shown in Fig. 6, during each current pulse, the battery is first charged or discharged with 1*C* (*C* rate, defined as a charge or discharge rate equal to the capacity of a battery divided by 1 h) constant current for 6 min (10% interval of *SOC*) and then rested for 3 h. The battery *OCV* is measured at the end of the rest period.

To identify the PDF of the battery, the charging first order reversal (FOR) branches are tested and the method of Everett function is used. In a charging FOR test, the cell is first charged to 100% *SOC* and then discharge to the full discharge state. Then the cell is charged to 100% *SOC* again and discharge to 10% *SOC*. The charge-discharge loop repeats until

the discharge point reaches 90% *SOC*. The detailed procedure of the charging FOR test is shown in Fig. 7. With the tested data of the charging FOR test procedure, the PDF can be identified with the Everett function method, which is very easy to implement. The detail of this method can be found in Ref. [21].

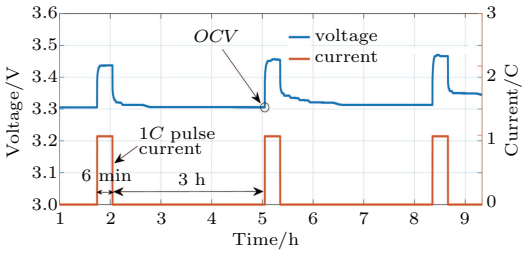


Fig. 6. (color online) Example of pulse current test.

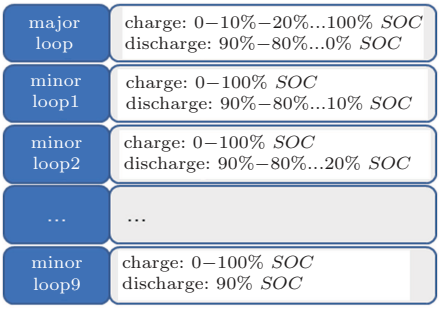


Fig. 7. (color online) Diagram of the charging FOR branch test.

To verify the PDF identified with the charging FOR branch test, another hysteresis input beyond the training data of the FOR branch is designed, which is named loop H2. To examine the performance of the tested PDF in the whole *SOC* range, loop H2 is designed to be comprised of three minor loops that spread at the high, medium and low location of the whole *SOC* range. Figure 8 shows the diagram of loop H2.

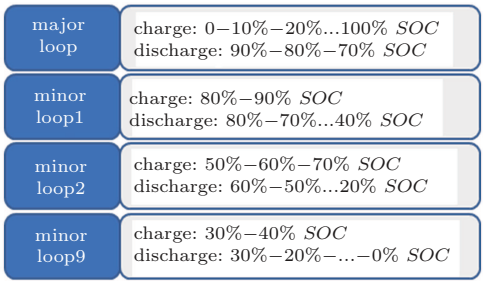


Fig. 8. (color online) Diagram of loop H2.

3.3. *OCV* estimation experiment with RDPM

To model the *SOC*–*OCV* relationship of LiFePO4 battery online with RDPM, the battery *SOC* is chosen as an input variable and *OCV* is chosen as the output variable. A very important issue for RDPM is to determine the value of N (the Preisach plane is divided by $N \times N$ parts). A larger value of N leads to a more accurate modeling result but will increase the duration time of experiment. In this paper, N is chosen to be 10 with considering the balance of model accuracy and experiment duration time. The flow chart of the RDPM estimation experiment is schematically illustrated in Fig. 9.

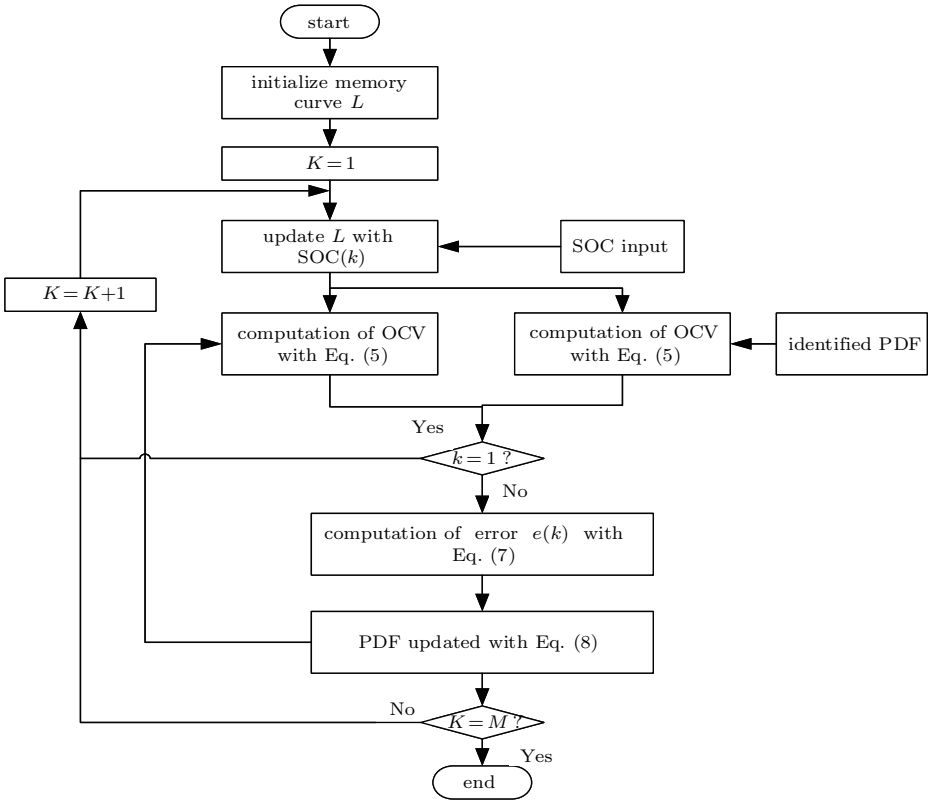


Fig. 9. Flow chart of the RDPM estimation process.

4. Effectiveness and performance of RDPM

4.1. Verification of DPM

The PDFs identified in the experiments with the charging FOR branches are shown in Figs. 10(a) and 10(b). It can be observed from Fig. 10 that the values of the hysterons distributed near the border of the Preisach triangle are apparently larger than the ones in the central area. This is possibly caused by the "flat" shape and small hysteresis value of the *SOC–OCV* curve of LiFePO4 battery.

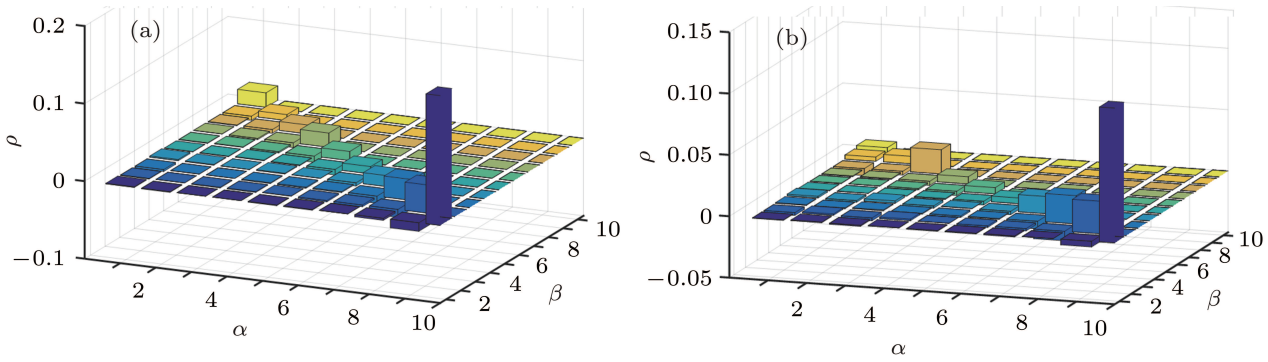


Fig. 10. (color online) Tested PDFs of cell A and cell B. (a) PDF of cell A; (b) PDF of cell B.

Model verification experiments are carried out for both cell A and cell B to verify the performance of DPM under the extended input beyond the training data. Loop H2 is used as the verification hysteresis input and the *OCV* relative error is used to judge the accuracy of the estimated PDF. The *OCV* relative error is computed from

$$err = (\widehat{OCV} - OCV)/\Delta OCV, \tag{9}$$

where $\widehat{OCV}$ is the estimated *OCV*, *OCV* is the tested *OCV*, and ΔOCV is the difference between the maximum and minimum *OCV* value of each cell. Figure 11(a) and 11(b) compares the estimated *OCV* curve and the measured *OCV* curve. Figure 11(c) and 11(d) show the scatter diagrams of the *OCV* estimation error. It can be seen that for both cells, the estimated curve fits the measured curve well.

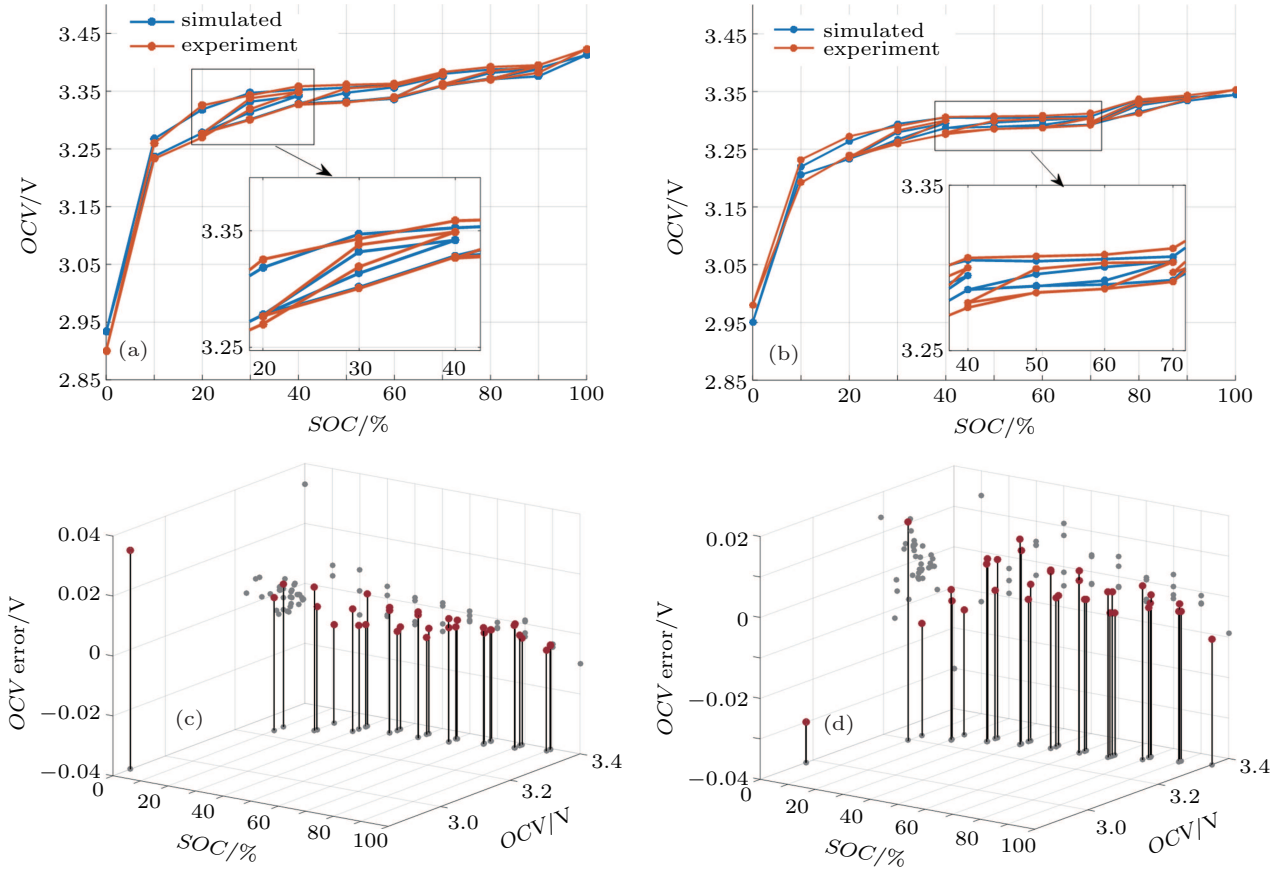


Fig. 11. (color online) Experimental *SOC–OCV* curve versus *SOC–OCV* curve simulated with DPM. (a) *SOC–OCV* curve of cell A; (b) *SOC–OCV* curve of cell B; (c) *OCV* estimation error scatter diagram of cell A; (d) *OCV* estimation error scatter diagram of cell B. The insert show the linear amplification.

To test the robust of DPM when the PDF of the cell changes, the PDF of cell A is used to estimate the *OCV* value of cell B with loop H2 used as the input to simulate the change of the cell hysteresis characteristic. The estimated *OCV* curve and the measured *OCV* curve are shown in Fig. 12(a) and the scatter diagram of the *OCV* estimation errors are shown in Fig. 12(b). It can be seen that there is an obvious deviation of the estimated curve from the measured curve. The root mean square (RMS) value and peak value of the relative estimation error are also listed in Table 2, and it can be observed that the estimation precision decreases obviously as the PDF of the cell changes.

Table 2. Comparisons between RMS and peak value of the *OCV* relative errors estimated with DPM and RDPM.

	RMS value		Peak value	
	DPM	RDPM	DPM	RDPM
Cell A	1.8%	1.8%	6.6%	6.6%
Cell B	1.7%	1.7%	6.0%	6.0%
PDF changed	6.5%	1.8%	14.5%	6.6%

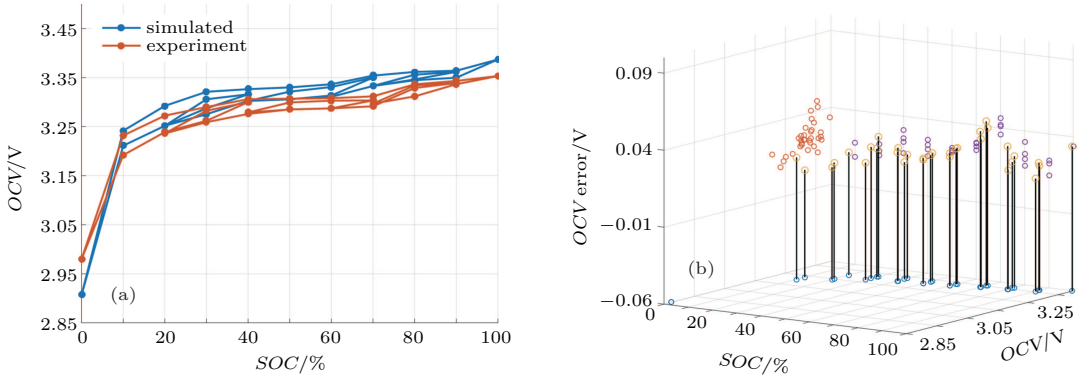


Fig. 12. (color online) DPM modeling results when cell PDF changes. (a) Comparison result of *SOC*–*OCV* curve; (b) *OCV* estimation error scatter diagram.

4.2. Verification of RDPM

The online identification of the PDF is carried out by using the loop H3 as an input and the PDF of Cell A is used as a reference PDF to calculate the reference *OCV* in the RDPM process. The initial value of the estimated PDF is set to be zero. The Preisach distributions taken for example at the recursive steps of $n = 50$, 100, 150, and 1000 in the estimation process are shown in Fig. 13. It can be seen that as the estimation proceeds, the estimated PDF converges to the reference PDF of cell A. The cumulative absolute error between the estimated PDF and the reference PDF is used to illustrate the performance of RDPM and calculated from

$$E = \sum_{\alpha=1}^{10} \sum_{\beta=1}^{\alpha} |\omega(\alpha,\beta) - \hat{\omega}(\alpha,\beta)|. \tag{10}$$

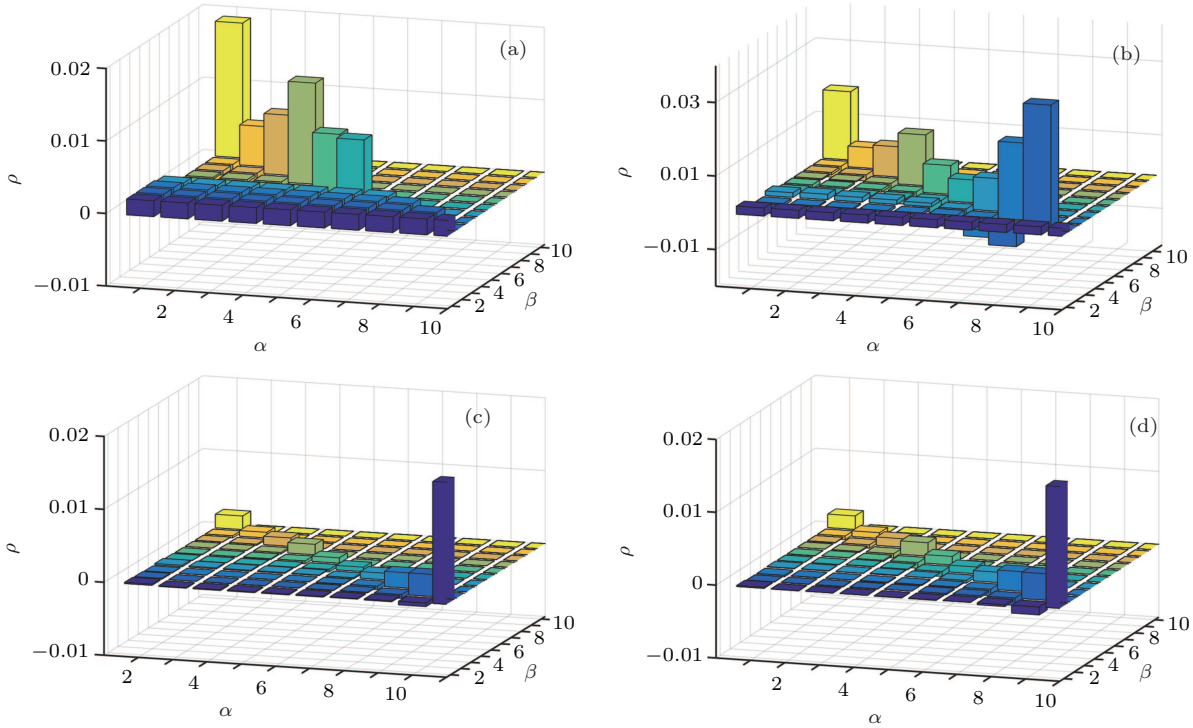


Fig. 13. (color online) Estimated PDF at the recursive steps of (a) $n = 50$; (b) $n = 100$; (c) $n = 150$; (d) $n = 1000$.

The resulting cumulative absolute error in the RDPM process is shown in Fig. 14. As illustrated in Fig. 14, the estimated PDF converges fast at the early period of the estimation process and as the estimated PDF gets very close to the reference PDF, the convergence speed slows down. The comparison between the results of the estimated *OCV* and the reference *OCV* in the estimation process as well as the logarithm of the *OCV* estimation error are shown in Fig. 15. It can be observed that the estimated *OCV* and the reference *OCV* will be in relatively high accordance as the estimation process proceeds.

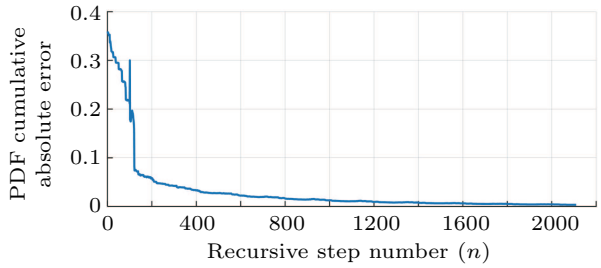


Fig. 14. (color online) Cumulative absolute error between the estimated PDF and the reference PDF.

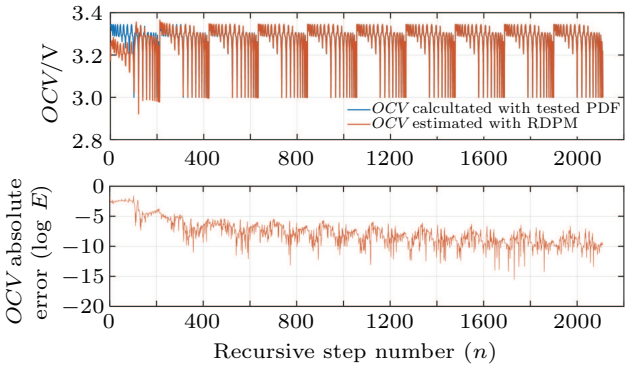


Fig. 15. (color online) Comparison between estimated *OCV* and reference *OCV* in the estimation process as well as the logarithm of the *OCV* estimation error.

To further verify the performance of RDPM, the PDF acquired from the RDPM process is used to model the *SOC*–*OCV* relationship under the input of loop H2 and the modeling result is compared with the result in Subsection 4.1. Figure 16 shows the variation of the RMS relative *OCV* estimation error in the estimation process. It can be seen that at the beginning, the estimation error is very large as the estimated PDF is very different from the reference PDF, but as the estimation process proceeds, the estimation error decreases fast and finally keeps stable around 1.8%. Table 2 shows the comparison between the RMS and peak value of the *OCV* relative errors estimated with DPM and RDPM respectively. The comparison result shows that compared with the traditional DPM method, the adopted RDPM method can significantly increase the *OCV* estimation precision as the cell *OCV* characteristic changes and the *OCV* estimation accuracy is almost not influenced by the change of the cell *OCV* characteristic when the RDPM method is used.

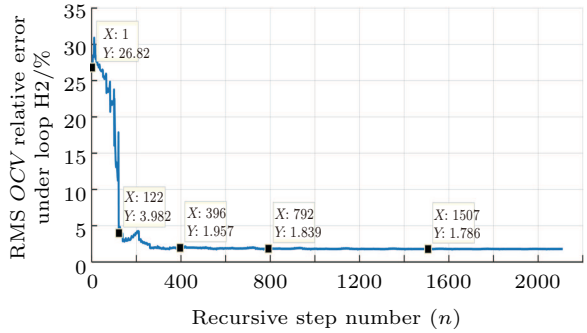


Fig. 16. (color online) Variation of RMS relative *OCV* estimation error with recursive step number the RDPM estimation process.

4.3. Influence of initial estimation PDF

The influence of initial PDF on the performance of RDPM is also studied. In this condition, cell B is used as a reference cell and the initial PDF is set to be the PDF of cell A and zero. Loop H3 is still used as the hysteresis input. The comparison result of the PDF cumulative absolute error is shown in Fig. 17. It can be seen that at the beginning, the initial PDF of cell A leads to a smaller estimation error. However, as the estimation process proceeds, the PDF estimated with the initial PDF of zero converges faster to the reference PDF, and when the recursive step number n reaches around 150, the two curves become almost identical. The estimated *OCV* absolute error illustrated in Fig. 18 also indicates the same conclusion. From the comparison result it is known that the convergence situation of RDPM depends mainly on the recursive step number and the initial estimation PDF only affects the early period of the RDPM estimation process but does not affect the final estimation result.

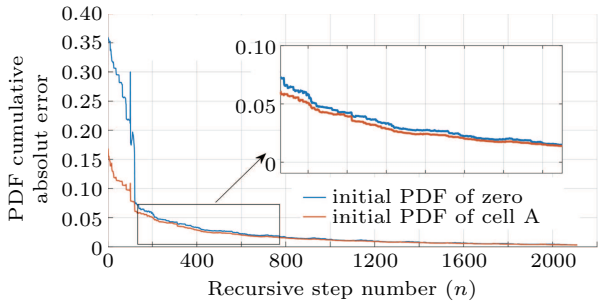


Fig. 17. (color online) Variations of PDF cumulative absolute error with recursive step number for different initial PDF values. The insert shows the linear amplification.

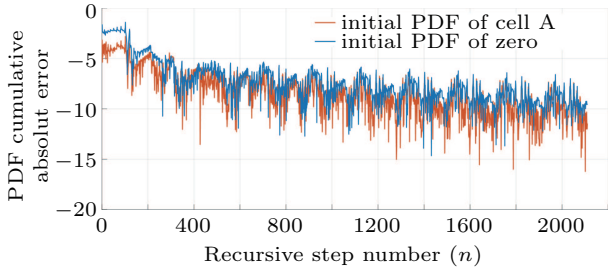


Fig. 18. (color online) Variations of *OCV* absolute error with recursive step number for different initial PDF values.

4.4. Performance of RDPM considering reference *OCV* uncertainties

In actual usages, the value of *OCV* cannot be measured directly and is usually estimated with battery models. However, as there exist errors in model parameters, the estimated *OCV* usually deviates from the true *OCV*. To testify the reliability of the proposed RDPM algorithm under the existence of reference *OCV* uncertainty, random errors with 5-mV and 10-mV magnitude (the mean values are both zero) are added to the reference *OCV* in the estimation process. Figure 19 shows the variations of PDF cumulative absolute error with recursive step number for different random *OCV* errors. It can be observed that at the beginning of the estimation process, the influences of different reference *OCV* are almost negligible. However, as the step number increases and the estimated PDF converges, the PDF error estimated with inaccurate *OCV* stops decreasing and began to fluctuate. It can be further observed that the PDF error is bigger in the condition of a larger reference *OCV* error. This is caused probably by the direct dependence of the update scheme on the reference *OCV*. Figure 20 compares the RMS *OCV* relative error under the input of loop H2. It can be seen that the estimation result with 5-mV magnitude random error is almost the same as the result of accurate *OCV*, while the result with 10-mV magnitude random error has a larger estimation error. However, even in the case of 10-mV reference *OCV* error, the estimated RMS *OCV* relative error stays below 3% for most of the cases. This comparison result shows that the RDPM algorithm has a good performance in the case of reference *OCV* uncertainty.

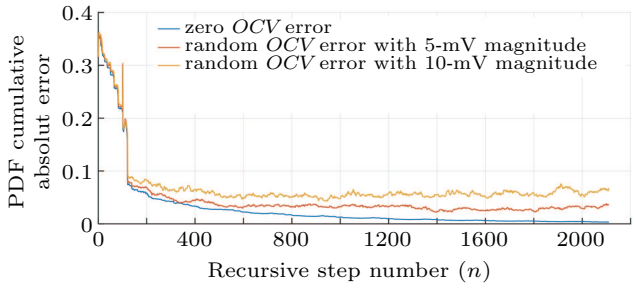


Fig. 19. (color online) Variations of estimated PDF cumulative absolute error for different reference *OCV* uncertainties.

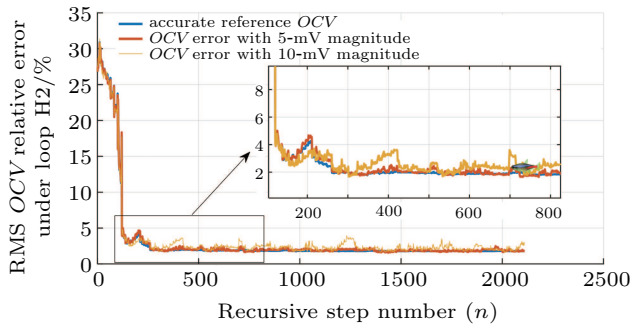


Fig. 20. (color online) Variations of RMS *OCV* relative error with recursive step number for different reference *OCV* uncertainties. The insert shows the linear amplification.

5. Conclusions

This paper focuses on the modeling of LiFePO4 battery *OCV* hysteresis. The RDPM algorithm which is originally used in the magnetic material hysteresis characterization is used for the hysteresis modeling of LiFePO4 battery. The experimental result shows that the proposed method can significantly improve the accuracy of LiFePO4 battery *OCV* hysteresis modeling when the battery *OCV* characteristic changes. Besides, the influence of initial estimation PDF and reference *OCV* uncertainties are also discussed. The simulation and experimental results show that the proposed method has a stable working performance under different initial estimation PDFs and reference *OCV* uncertainties. By means of this research, battery parameter and state estimation technologies such as battery ECM and Kalman filter can further be combined with to realize a more accurate state estimation of LiFePO4 battery. The proposed method shows a promising performance that will benefit the state estimation of LiFePO4 battery.

References

[1] Wang D, Guan, X H, Wu J, Li P, Zan P and Xu H 2016 *IEEE Trans. Smart Grid* **7** 1762
[2] Gan L, Ufuk T and Steven H L 2013 *IEEE T Power Syst.* **28** 940
[3] Pellegrino and Gianmario 2013 *IEEE T. Ind. Electron.* **59** 803
[4] Ansean D, Gonzalez M, Garcia M V 2015 *IEEE T Ind. Appl.* **2** 1855
[5] Yu Z H, Tian J R and Song Y R 2014 *Chin. Phys. B* **23** 094206
[6] Liu G Q and Ying H P 2014 *Chin. Phys. B* **23** 050502
[7] Zhao S M and Zhuang P 2014 *Chin. Phys. B* **23** 054203
[8] Shi S Q, Gao J, Liu Y, Zhao Y, Wu Q, Ju W W, Ouyang C Y and Xiao R J 2016 *Chin. Phys. B* **25** 018212
[9] Jiang Y H, Ai L J, Ming C Y, Du S L and Li S G 2017 *Acta Phys. Sin.* **66** 118202 (in Chinese)
[10] Huang L L and Jian Y 2015 *Acta Phys. Sin.* **64** 108202 (in Chinese)
[11] Kasavajjula U S, Wang C and Arcea P E 2008 *J. Electrochem. Soc.* **155** 866
[12] Plett G L 2004 *J. Power Sources* **134** 262
[13] Baronti F, Zamboni W, Femia N and Roncella R 2013 *IECON* 2013 – 39*th Annual Conference on IEEE Industrial Electronics Society*, 2013, Vienna, Austria, p. 6726
[14] Huria T, Ludovici G and Lutzemberger G 2014 *J. Power Sources* **249** 92
[15] Verbrugge M and Tate E 2004 *J. Power Sources* **126** 236
[16] Thele M 2008 *J. Power Sources* **175** 635
[17] Kim J, Seo G S and Chun C 2012 *IEEE International Electric Vehicle Conference (IEVC)*, 2012 p. 1
[18] Windarko N A and Choi J 2009 31*rt International Telecommunications Energy Conference*, 2009, p. 1
[19] Windarko N A and Choi J 2010 *J. Power Electron.* **10** 181
[20] Trapanese M, Franzitta V and Viola A 2013 *Twenty-Eighth Annual IEEE Applied Power Electronics Conference and Exposition (APEC)*, 2013, p. 2773
[21] Preisach F 1935 *Z. Phys.* **94** 277
[22] Tang X D 2008 *International Conference on Prognostics and Health Management*, 2008, p. 1
[23] Tjandra R 2014 *Transportation Electrification Conference and Expo (ITEC)*, 2014, p. 1
[24] Baronti F, Femia N and Saletti R 2015 *Journal of Energy Storage* **4** 51
[25] Zhu L T, Sun Z C, Dai H F and Wei X Z 2015 *J. Appl. Energy* **155** 91
[26] Mayergoyz I D 1986 *Phys. Rev. Lett.* **22** 603
[27] Ruderman M 2013 *J. Magn. Magn. Mater.* **348** 22